Neural Electrode Array Based on Aluminum: Fabrication and Characterization

Alexandre Coumiotis Moreira Peixoto, Sandra Beatriz Gonçalves, Alexandre Ferreira Da Silva, Nuno S. Dias, and J. Higino Correia, *Member, IEEE*

***Abstract*— A unique neural electrode design is proposed with 3 mm long shafts made from an aluminum-based substrate. The electrode is composed by 100 individualized shafts in a 10 × 10 matrix, in which each aluminum shafts are precisely machined via dicing-saw cutting programs. The result is a bulk structure of aluminum with 65° angle sharp tips. Each electrode tip is covered by an iridium oxide thin film layer (ionic transducer) via pulsed sputtering, that provides a stable and a reversible behavior for recording/stimulation purposes, a 40 mC/cm^2 charge capacity and a 145 Ω impedance in a wide frequency range of interest (10 Hz–100 kHz). Because of the non-biocompatibility issue that characterizes aluminum, an anodization process is performed that forms an aluminum oxide layer around the aluminum substrate. The result is a passivation layer fully biocompatible that furthermore, enhances the mechanical properties by increasing the robustness of the electrode. For a successful electrode insertion, a 1.1 N load is required. The resultant electrode is a feasible alternative to silicon-based electrode solutions, avoiding the complexity of its fabrication methods and limitations, and increasing the electrode performance.**

***Index Terms*— Invasive electrode, recording, stimulation, iridium oxide, aluminum, electrode array, sharp tips.**

I. Introduction

THE ability to access deep areas of the brain to record the electrical activity or to perform functional stimulation is a key feature to understand the neurophysiological processes and to restore nervous system's lost functionalities [1].

This became possible with the development of neural interfaces. They have been designed to establish a connection between the neurons (electrically active cells of the nervous system) and the electronic system that handles the biopotentials. One may find neural interfaces in limb prostheses for spinal cord injury and stroke, bladder prostheses, cochlear auditory prostheses, retinal and cortical visual prostheses, cortical recording for cognitive control of assistive devices, and deep brain stimulation for essential tremor in Parkinson's disease [2].

In order to establish a neural interface it is necessary to transduce a signal between the electrical domain (electronic circuit) to the biological domain (neurons) and vice-versa. This is accomplished using an electrode in which a charge transduction occurs between the electrons species of the electrode material and the ions species of the electrolyte.

Nonetheless, the neural electrodes differ from the standard biopotentials electrodes. The neural solutions are known to be invasive, of small size, and multichannel. One can define a set of features that neural electrodes should comply with, namely: electrodes should remain stable for long periods of time; its cross section should be as small as possible in order to displace or damage as little tissue as possible during insertion; and the implantable electrode should have a large density of transduction ports to interface with different neurons.

In this neurophysiologic field, two neural electrodes designs stand out: the Michigan probe [3] and the Utah probe [4].

The Michigan probe is a multi-point electrode type. The electrode is composed by an array of shafts that in each one, there are several transduction ports individually addressable. The result is a map of the electrical activity at multiple depths of the brain (along the shaft depth). However, this electrode designs presents a fabrication process highly complex with a low production yield. Furthermore, the fragility of each shank leads to breaks during the insertion, and consequently tissue damage [5].

The Utah probe is characterized by an array of shafts, with a single transduction point at the shafts' tip. Its fabrication process is based on the micromachining of silicon wafers via physical and chemical processes. Depending on the wafer (if type p or n), exotic processes are required as thermomigration to establish conductive paths across the wafer [6], or instead, glass fusion to isolate each shaft from the surrounding shafts in the same array [7]. Either way, the Utah's fabrication processes have strict requirements as high temperature ovens for fusing glass or even specially designed ovens for the thermomigration technique. Moreover, it requires the use of wet-etching to sharpen the shafts' tips. Overall, these mentioned processes end up resulting in a low reproducibility rate.

Manuscript received December 14, 2012; revised June 3, 2013; accepted June 5, 2013. Date of publication June 19, 2013; date of current version July 30, 2013. The work of A.C. Peixoto was supported in part by the Portuguese Foundation for Science and Technology under Grant SFRH/BD/89509/2012, and the FCT with the reference Project FCOMP 01 0124-EDER-010909 under Grant FCT/PTDC/SAU-BEB/100392/2008. The associate editor coordinating the review of this paper and approving it for publication was Prof. Carlo Morabito.

A. C. M. Peixoto, S. B. Gonçalves, and J. H. Correia are with the Department of Industrial Electronics, University of Minho, Guimaraes 4800-058, Portugal (e-mail: alexandre.peixoto@dei.uminho.pt; sbeatriztg@gmail.com; higino.correia@dei.uminho.pt).

A. F. Da Silva is with the MIT Portugal Program, School of Engineering, University of Minho, Guimarães 4800-058, Portugal (e-mail: asilva@dei.uminho.pt).

N. S. Dias is with the Life and Health Sciences Research Institute, University of Minho, Braga 4710-057, Portugal, and also with DIGARC, Portugal Polytechnic Institute of Cavado and Ave, Barcelos 4750-810, Portugal (e-mail: ndias@dei.uminho.pt).

Color versions of one or more of the figures in this paper are available online at http://ieeexplore.ieee.org.

Digital Object Identifier 10.1109/JSEN.2013.2270034

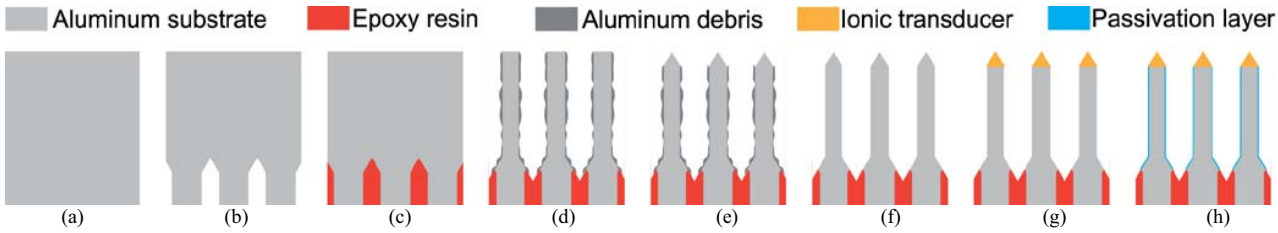

Fig. 1. Fabrication steps: (a) Aluminum substrate; (b) Pads region delimitation; (c) Pads' groves filling with epoxy resin; (d) Shafts cutting stage; (e) Shafts sharpening; (f) Shafts cleaning via etching stage; (g) IrO2 thin-film deposition at the shafts' tips; (h) Electrode passivation.

Moreover, in both approaches a maximum penetration depth of 1.5 mm has been reported [5].

A new fabrication approach is proposed, using a different bulk material for the electrode substrate, different techniques that provide high-production yield, reproducibility, and an electrode with 3 mm range of depth. The presented electrode design is made from an aluminum-based bulk substrate, with iridium oxide (IrO2) as ionic transducer at each shaft tip and coated with a passivation layer of aluminum oxide. The fabrication steps are described in detail and the electrode is fully characterized (morphologically, mechanically and electrically).

II. Electrode Design

When designing a neural electrode, it is important to consider the need for a stationary solution, capable of providing high-spatial resolution interface with the neurons [8] and reaching several points of interest [9] with increasing penetration depths. Moreover, due to the invasive nature of neural electrodes, it becomes imperative, for Chronic applications, to ensure mechanical, chemical and electrical long-term stability.

The electrode requirements define the constraints regarding materials to be used, fabrication processes and overall electrode shape.

The single-channel matrix design has proven to be the most adequate design for implantable neural electrodes [10] due to its robustness and flexibility.

The fabrication of the electrode should be compatible with large-scale manufacturing solutions and therefore, a simple and highly reproducible process was sought. The two major techniques selected were a combination of dicing with wet-etching. By using the dicing with a special designed saw that presents a wedge shape, it would be possible to establish a cutting plan that would create the sharp tips and the long shafts. The wet-etching would only be applied for cleaning purposes, removing all the scrap material that piles up in the cuts.

In combination with the fabrication technique, a different bulk material was selected. Instead of using the standard silicon wafer, it was decided to use an aluminum piece as bulk. Aluminum, being a ductile and easy to machine material, offers some advantages over silicon commonly used in the production of neural prosthesis. Aluminum is a natural good conductor, offering very low resistivity (28.2 nΩ.m) [11]. This characteristic offers an electrical advantage over doped silicon, which has been reported to have a resistivity at best of 50,000 nΩ.m [12], which is a difference of 3 orders of magnitude between aluminum and doped silicon.

However, aluminum has two main drawbacks: non-biocompatibility and low Young's modulus. Although aluminum is used as body material and conductive channel for the biopotentials, it is required to coat/passivate it not only to ensure that no aluminum is in contact with neural tissue due to toxicity reasons but also to guarantee that only the tip is performing the signal interface with the neurons and not the entire shaft. The aluminum ductility may be a concern, depending on the aspect ratio of the fabricated shaft. But, since one desires long shafts with low widths, the ductility may induce the shaft to bend during the insertion. In order to avoid these two issues, an anodization procedure is proposed. It is possible to anodize the aluminum, creating an external coating of aluminum oxide. The result is a covering that not only is biocompatible and therefore solving the cytotoxicity issues but that also has a superior Young's modulus compared to the aluminum that enhances the structural robustness of the entire electrode [13], [14].

It is necessary to select the material to perform the ionic transduction at the shaft's tip site as neither aluminum nor doped silicon are able to perform the charge transfer at the electrode-electrolyte interface. There are several suitable materials, which include silver/silver chloride (Ag/AgCl) [15], titanium nitride (TiN), platinum (Pt) [16] and iridium oxide (IrO2) [17]. Nonetheless, IrO2 has been proven to be one of the most promising and preferred materials for electrodes [18], [19] due to its high charge delivery capacity, low constant impedance over the entire frequency range for neural stimulation and biocompatibility [20].

III. Electrode Fabrication

The fabrication procedure for the proposed electrode design (Figure 1) uses a combination of different techniques, namely: dicing, polymer deposition, wet-etching and electrolytic passivation.

The dicing stage comprises a cutting plan to delineate and to shape the wafer in order to establish the structural shape of the intended electrode array matrix. The cutting plan is divided into four sub-stages, all of them performed on a Disco DAD 2H/6T dicing machine, equipped with Disco ZHDG blades capable of performing 3 mm deep, 0.250 mm wide cuts and V-shaped grooves. The substrate was an aluminum square chunk, 99 % pure, 10 mm wide and 5 mm thick.

The first series of cuts is performed on the backside of the aluminum chunk (Figure 1b) and intends to outline each

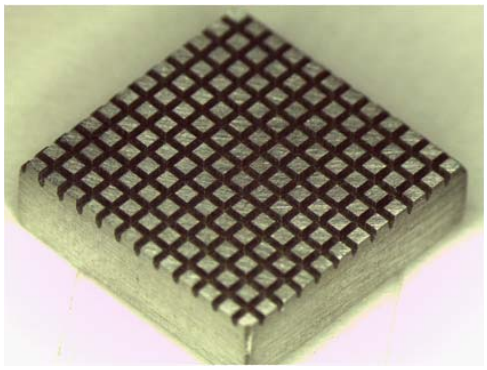

Fig. 2. Definition of the pads regions on the aluminums wafer's backside.

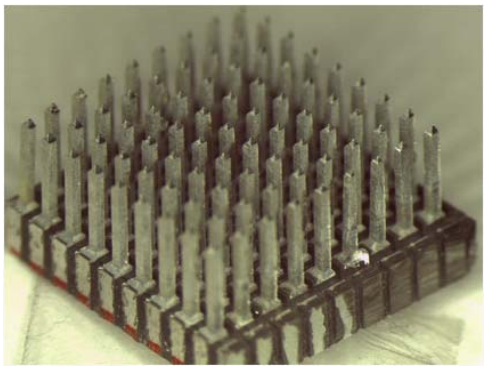

Fig. 3. Electrode matrix structure after the etching stage.

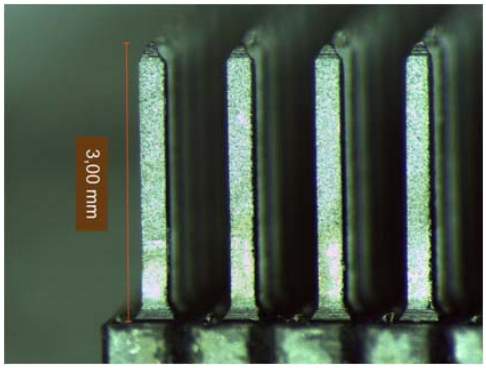

Fig. 4. Detailed view of a set of the 3 mm long shafts.

pad Region. These pads will be the connecting sites for interrogating each electrode tip. The cuts have a grid profile, in which the cut is 2.5 mm deep and 1 mm spaced (Figure 2).

Afterwards, the resultant cavities are filled with an epoxy-resin (Figure 1c) that will serve as electrical insulation between electrodes in the final structure and will also be the structural element that provides structural integrity to the electrode matrix and keep it as a whole and single component. The polymer is slowly laid over the backside center, forcing the air inside the groves to be pushed out as the polymer fills the grooves. After the polymer cure, the backside surface is grinded and polished to remove the excess of polymer, resulting in a smooth surface.

The epoxy-resin was the selected material due to its high-level of adhesion to aluminum and chemical resistance.

With the backside defined, the fabrication steps are now dedicated to creating the sharp shafts (Figure 1d–f).

First, a cut plan is performed to machine a matrix of 3 mm high and 350 μm wide pillars (Figure 1d). The space between pillars is in accordance to the distance between pads. In this case, a 1 mm space was set in order to create a 10 $\times$ 10 electrode matrix in a 10 mm wide square aluminum chunk. Higher electrode densities are possible but it is necessary to adjust the spacing value.

After the first stage of cuts, the shafts present a straight square profile that need to be sharpened to facilitate the implantation. The shafts are sharpened by passing the cutting blade on the top of the pillar, near its edge.

After the cut, a large amount of aluminum debris piles in the space between the pillars and in order to clean it, the electrode is immersed on type-A aluminum etchant at 50 °C for 30 minutes (Figure 1f) [21]. As the etchant also attacks the shafts' aluminum, it is therefore necessary to take it into account and have a wider shaft width that will be thinned when immersed in the etching bath. The result is a clean electrode matrix structure of high-aspect ratio shafts as shown in Figure 3. A detailed view of the final shafts is showed in Figure 4.

At this point the electrode's shafts are not yet functionalized. So far, one has the main electrode body fully conductive but not able to perform the charge transduction.

In order to deposit the ionic transducer at the shafts' tips, an aluminum foil was pressed against them exposing only the very tips. This foil is placed with the aid of two fiber glass sheets. The upper sheet has 500 μm holes with 1 mm spacing between them, allowing the shafts to pass through it while the lower sheet has no holes. Controlling the distance between these two sheets there are four precision screws and bolts at each corner. By placing the foil below the upper sheet and controlling the number of turns in each nut, the exposed region is precisely controlled.

Prior to the iridium oxide deposition, a thin layer of 50 nm titanium (Ti) is deposited by DC sputtering. The Ti layer will promote the adhesion of the iridium film to the aluminum. The iridium oxide is deposited by pulsed Sputtering in a 3.5 sccm oxygen flow at 180 W (50 kHz).

In the last fabrication stage, the aluminum shafts need to be passivated via anodizing. The process is performed by submersing the shafts in a sulfuric acid solution while injecting a 13 mA/cm^2 current density through the electrode shafts (anode) and a platinum electrode (cathode).

A close up image of the aluminum oxide protective layer can be seen on Figure 5.

IV. Results

A. Morphology

Figure 6 shows the main measurements that define each shaft tip. The shaft features include a 3 mm high and 250 μm wide shank, with a square-base pyramidal shape tip with a 65° vertex. In a population of 69 samples the average angle was 65° with a standard deviation of 5.67°, while the average

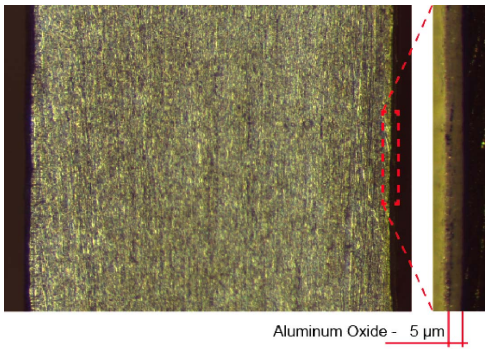

Fig. 5. Anodized shafts cross-section with a detailed view of the aluminum oxide protective layer.

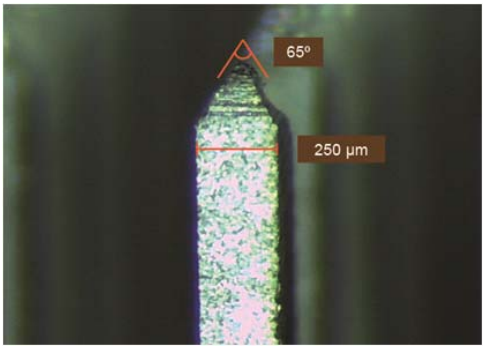

Fig. 6. Detailed view of single shaft tip.

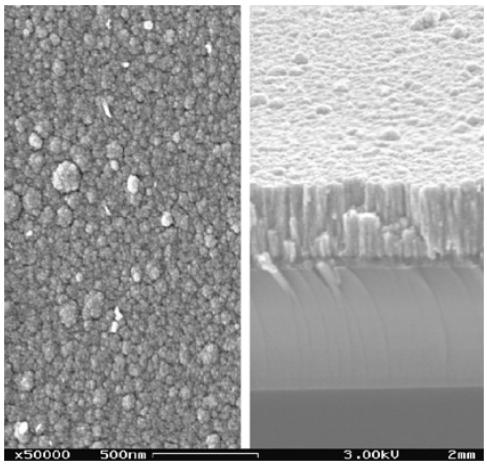

Fig. 7. SEM image of the IrO2 thin-film (top and cross-section view).

height was 3 mm with a standard deviation of 50 μm. The average tip radius was of 9 μm.

The shaft base is an aluminum block of 0.7 $\times$ 0.7 $\times$ 0.2 mm^3 for a 10 $\times$ 10 electrode matrix in a 10 mm square substrate.

Figure 7 shows in detail the surface and cross-section of the iridium oxide thin-film deposited at the shaft tip. The images were obtained by scanning electron microscope technique and it is possible to identify a grainy structure with a coherent morphology.

B. Mechanical

The mechanical analysis focused on the load required to implant the electrode and on the electrode robustness. The tests

Fig. 8. Mechanical test arrangement.

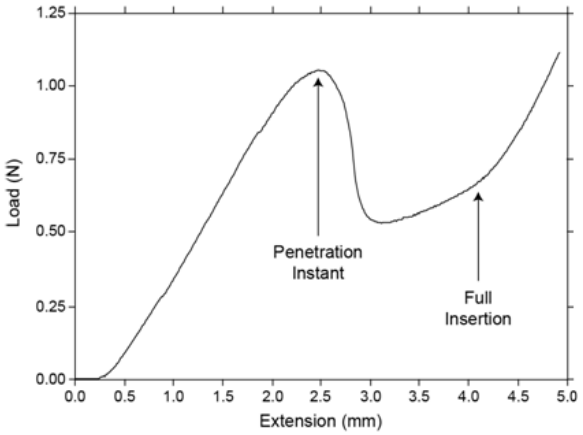

Fig. 9. Electrode's implantation mechanical response.

were performed on a Hounsfield H 100 KS dynamometer equipped with a 100 N load cell and capable of a resolution of 10 mN. The neural tissue mechanical properties were mimicked via agar-agar gel (1% solution) [22]. Figure 8 shows the setup arrangement for the implantation analysis.

The crosshead was set to move at a constant displacement rate of 30 μm/s towards the gel (compressive load), while the required load was being acquired.

The obtained plot (Figure 9) shows a load increase on the initial stage while still subjected to the material gel resistance up to the moment where the electrodes' tips are able to pierce the gel. From this moment beyond there is a fast decrease of the required load to fulfill the entire electrode implantation. This suggests a bed-of-nails effect during insertion. On the final stage there is a slightly higher increase slope related to the material resistance when the electrode was already fully inserted and the crosshead continued the displacement.

The required load, according to the obtained data, is approximately 1.13 N with a 13 % variation among samples. These values are similar to results reported in other studies [23].

The electrodes were also removed from the gel after the test to evaluate their integrity and effect on the gel. None of the tested samples showed any sign of break or bended shafts. The pierced holes on the gel seemed to partially recover from insertion.

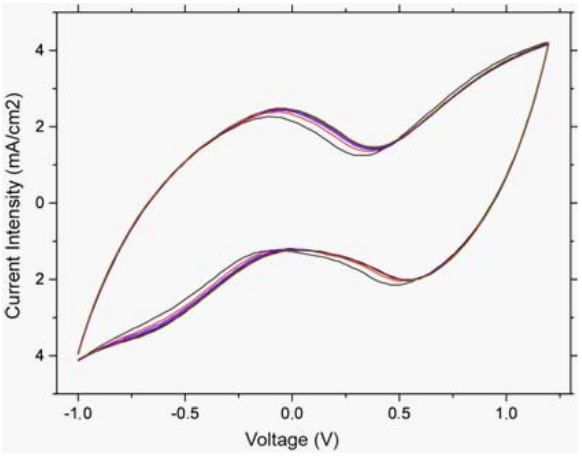

Fig. 10. Cyclic voltammetry measurements for different activation cycles.

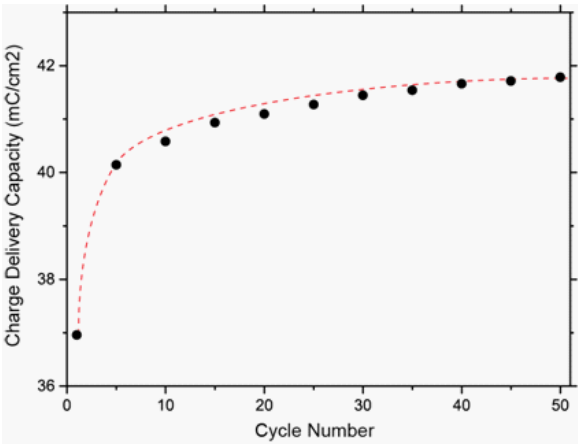

Fig. 11. Charge delivery capacity in dependence of the cycle number.

C. Electrical

The electrochemical analysis of the electrodes were performed on a Gamry Reference 600^{TM} Potentiostat/ Galvanostat. In an electrochemical cell, with a NaCl solution (0.9 % by weight), the thin-film of IrO2 that performs the electrode-electrolyte interface underwent cyclic voltammetry and impedance analysis.

The cyclic voltammogram (Figure 10) shows a reversible behavior, with minimum changes after several activation cycles. The reversibility of the process enables the electrode to be safely used for stimulation purposes.

Figure 11 shows how the charge delivery capacity changes along the activation cycles of the electrode, providing a look on how the electrode would perform along its lifecycle. Due to the electrochemical reactions occurring in the surface of the electrode its structure is modified resulting in this variation. The first cycles led to a fast increase of charge delivery capacity, which gradually reaches a plateau value.

The general shapes of the impedances before and after activation of 50 cycles are shown in the *Bode* plot of Figure 12. The cutoff frequency which represents the transition from the capacitive region to the resistive region, shifts to lower frequencies with activation. Successive activation cycles move the cutoff frequency further to lower frequencies but, the effects are not as pronounced.

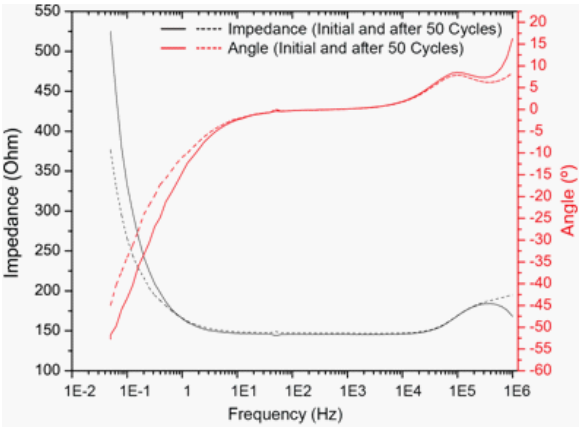

Fig. 12. Bode plot before and after activation with 50 cycles.

By lowering the cutoff frequency, the electrode gains a wider frequency range of low impedance useful for functional electro-stimulation. This way, the diffusion control plays a slighter role in impedance behavior of activated samples, meaning that, at lower frequencies, the electrode impedance is dominated by the double layer capacitance [24].

On Figure 12's secondary axis is possible to identify the behavior of the sample according to the signal frequency. For frequencies up to 100 Hz, the sample presents a capacitive component, and above 10 kHz it has a inductive component. But, for frequencies between 1 kHz and 10 kHz, the samples are purely resistive, since the *theta* is null, and in this frequency range, the impedance value is around 145 Ohm.

V. Conclusion

An electrode array with 3 mm long shafts made from an aluminum based substrate is fabricated.

The aluminum-based substrate proves to be a feasible alternative to silicon-based electrode solution by overcoming its limitations and its fabrication complexity. Nonetheless, it was necessary to establish a fabrication method capable of precise machining and to define solution to overcome the aluminum own limitations: biocompatibility and ductility.

The proposed fabrication procedure proved to be consistent and reproducible. Moreover, it enables the fabrication of shafts with heights well above the ones reported in bibliography.

The result was a robust invasive neural electrode matrix with 3 mm long shafts. The electrode can be easily implanted, requiring 1.1 N load at its base. The deposition of IrO2 films as the ionic transducer showed the required performance for its application, with a consistent reversible electrochemical behavior, and 40 mC/cm2 charge delivery capacity and a impedance of 145 Ohm in the same frequency range as the stimulation protocols.

Overall, the proposed electrode design becomes an eligible alternative for biopotentials recording and stimulation applications.

References

[1] B. S. Wilson and M. F. Dorman, "Interfacing sensors with the nervous system: Lessons from the development and success of the cochlear implant," *IEEE Sensors J.*, vol. 8, no. 1, pp. 131–147, Jan. 2008.

[2] S. F. Cogan, "Neural stimulation and recording electrodes," *Annu. Rev. Biomed. Eng.*, vol. 10, pp. 275–309, Jan. 2008.

[3] K. D. Wise, "Wireless integrated microsystems: Wearable and implantable devices for improved health care," in *Proc. Int. Solid-State Sens., Actuat., Microsyst. Conf.*, Jun. 2009, pp. 1–8.

[4] A. Sharma, L. Rieth, P. Tathireddy, R. Harrison, H. Oppermann, M. Klein, M. Töpper, E. Jung, R. Normann, G. Clark, and F. Solzbacher, "Long term in vitro functional stability and recording longevity of fully integrated wireless neural interfaces based on the Utah Slant electrode array," *J. Neural Eng.*, vol. 8, no. 4, p. 045004, Aug. 2011.

[5] M. Hajjhassan, V. Chodavarapu, and S. Musallam, "NeuroMEMS: Neural probe microtechnologies," *Sensors*, vol. 8, no. 10, pp. 6704–6726, 2008.

[6] P. K. Campbell, K. E. Jones, R. J. Huber, K. W. Horch, and R. A. Normann, "A silicon-based, three-dimensional neural interface: Manufacturing processes for an intracortical electrode array," *IEEE Trans. Biomed. Eng.*, vol. 38, no. 8, pp. 758–768, Aug. 1991.

[7] K. E. Jones, P. K. Campbell, and R. A. Normann, "A glass/silicon composite intracortical electrode array," *Ann. Biomed. Eng.*, vol. 20, no. 4, pp. 423–437, 1992.

[8] T. A. Fofonoff, S. M. Martel, N. G. Hatsopoulos, J. P. Donoghue, and I. W. Hunter, "Microelectrode array fabrication by electrical discharge machining and chemical etching," *IEEE Trans. Biomed. Eng.*, vol. 51, no. 6, pp. 890–895, Jun. 2004.

[9] R. Bhandari, S. Negi, L. Rieth, R. A. Normann, and F. Solzbacher, "A novel method of fabricating convoluted shaped electrode arrays for neural and retinal prostheses," *Sens. Actuators. A, Phys.*, vols. 145–146, nos. 1–2, pp. 123–130, Jan. 2008.

[10] R. A. Normann, "Technology insight: Future neuroprosthetic therapies for disorders of the nervous system," *Nature Clinical Pract. Neurol.*, vol. 3, no. 8, pp. 444–452, 2007.

[11] J. Cutnell and J. Kenneth, *Physics*, 3rd ed. New York, NY, USA: Wiley, 1995.

[12] R. Sharma, P. Tathireddy, S. Lee, L. Rieth, E. Bamberg, and A. Dorval, "Procedia engineering application-specific customizable architectures of Utah neural interfaces," *Engineering*, vol. 25, pp. 1–4, Feb. 2011.

[13] D. S. Finch, T. Oreskovic, K. Ramadurai, C. F. Herrmann, S. M. George, and R. L. Mahajan, "Biocompatibility of atomic layer-deposited alumina thin films," *J. Biomed. Mater. Res. Part A*, vol. 87, no. 1, pp. 100–106, Oct. 2008.

[14] K. E. Petersen, "Silicon as a mechanical material," *Proc. IEEE*, vol. 70, no. 5, pp. 420–457, May 1982.

[15] J. A. McLaughlin, E. T. McAdams, and J. Anderson, "Novel dry electrode ECG sensor system," in *Proc. 16th Annu. Int. Conf. IEEE Eng. Med. Biol. Soc.*, Nov. 1993, pp. 800–804.

[16] A. Ivorra, R. Gómez, N. Noguera, R. Villa, A. Sola, L. Palacios, G. Hotter, and J. Aguiló, "Minimally invasive silicon probe for electrical impedance measurements in small animals," *Biosens. Bioelectron.*, vol. 19, no. 4, pp. 391–399, Dec. 2003.

[17] S. F. Cogan, T. D. Plante, and J. Ehrlich, "Sputtered iridium oxide films (SIROFs) for low-impedance neural stimulation and recording electrodes," in *Proc. Conf. Proc. IEEE Eng. Med. Biol. Soc.*, vol. 6. Sep. 2004, pp. 4153–4156.

[18] R. B. McIntosh, P. E. Mauger, and S. R. Patterson, "Capacitive transducers with curved electrodes," *IEEE Sensors J.*, vol. 6, no. 1, pp. 125–138, Feb. 2006.

[19] J. P. Carmo, N. Sé. Dias, H. R. Silva, P. M. Mendes, C. Couto, and J. H. Correia, "A 2.4-GHz low-power/low-voltage wireless plug-and-play module for EEG applications," *IEEE Sensors J.*, vol. 7, no. 11, pp. 1524–1531, Nov. 2007.

[20] B. Wessling, W. Mokwa, and U. Schnakenberg, "RF-sputtering of iridium oxide to be used as stimulation material in functional medical implants," *J. Micromech. Microeng.*, vol. 16, no. 6, pp. 142–148, Jun. 2006.

[21] *Material Safety Data Sheet for Aluminum Etchant Type A*, Transene Co., Rowley, MA, USA, 1987.

[22] Z.-J. Chen, G. T. Gillies, W. C. Broaddus, S. S. Prabhu, H. Fillmore, R. M. Mitchell, F. D. Corwin, and P. P. Fatouros, "A realistic brain tissue phantom for intraparenchymal infusion studies," *J. Neurosurgery*, vol. 101, no. 2, pp. 314–322, 2004.

[23] M. Han, P. S. Manoonkitiwongsa, C. X. Wang, and D. B. McCreery, "In vivo validation of custom-designed silicon-based microelectrode arrays for long-term neural recording and stimulation," *IEEE Trans. Biomed. Eng.*, vol. 59, no. 2, pp. 346–354, Feb. 2012.

[24] B. Wessling, W. Mokwa, and U. Schnakenberg, "RF-sputtering of iridium oxide to be used as stimulation material in functional medical implants," *J. Micromech. Microeng.*, vol. 16, no. 6, pp. S142–S148, Jun. 2006.

Alexandre Coumiotis Peixoto received the Degree in electrical engineering and the master's degree in electrical engineering from the University of Trás-os-Montes e alto Douro, Vila Real, Portugal, in 2008 and 2010, respectively. He is currently pursuing a Ph.D. degree in biomedical engineering with the University of Minho, Guimarães, Portugal.

Sandra Beatriz Gonçalves received the Degree in biomedical engineering (Integrated Masters) with the major in medical electronics from the University of Minho, Guimarães, Portugal, in 2012. She is currently a Researcher with the University of Minho.

Alexandre Ferreira Da Silva graduated, in 2007, in Biomedical Engineering at University of Minho, Braga, Portugal. He obtained in 2011 the PhD degree in Leaders for Technical Industries, at the same institution, under the MIT-Portugal Program within the Engineering Design and Advanced Manufacturing (EDAM) focus-area. Presently, he is an assistant professor for the MIT Portugal's EDAM focus-area at University of Minho. His main research interests are related to the design and development of medical devices, and micro/nano fabrication technologies.

Nuno Sérgio Dias (S'06) received the Degree in industrial electronics and computers from the University of Minho, Braga, Portugal, in 2004, and the Ph.D. degree in industrial electronics from the University of Minho, Guimarães, Portugal, in 2009, in collaboration with the Center for Neural Engineering, Pennsylvania State University, State College, PA, USA. His Ph.D. thesis focused on Brain–Machine Interface Based on Biotelemetry and Dry Electrodes. He is currently a Post-Doctoral Researcher with the Life and Health Sciences Research Institute - ICVS, University of Minho. He is a member of the IEEE Industrial Electronics Society and the IEEE Engineering in Medicine and Biology Society.

José Higino Correia (S'96–M'00) received the Degree in physical engineering from the University of Coimbra, Coimbra, Portugal, in 1990, and the Ph.D. degree from the Laboratory for Electronic Instrumentation, Delft University of Technology, Delft, The Netherlands, in 1999, working in microsystems for optical spectral analysis. He is currently a Full Professor with the Department of Industrial Electronics, University of Minho, Braga, Portugal. He was the General-Chairman of Eurosensors in 2003 and MME in 2007. His current research interests include micromachining and microfabrication technology for mixed-mode systems, solid-state integrated sensors, microactuators and microsystems. He is a member of the IEEE Industrial Electronics Society.